Multiscale steady discrete unified gas kinetic scheme with macroscopic coarse mesh acceleration using preconditioned Krylov subspace method for multigroup neutron Boltzmann transport equation

Xiafeng Zhou[1,2,*] and Zhaoli Guo[2,†]

[1]*Department of Nuclear Engineering and Technology, School of Energy and Power Engineering, Huazhong University of Science and Technology, Wuhan 430074, China*

[2]*Institute of Interdisciplinary Research for Mathematics and Applied Science, School of Mathematics and Statistics, Huazhong University of Science and Technology, Wuhan 430074, China*

(Received 20 December 2022; accepted 28 March 2023; published 24 April 2023)

A multiscale steady discrete unified gas kinetic scheme with macroscopic coarse mesh acceleration [accelerated steady discrete unified gas kinetic scheme (SDUGKS)] is proposed to improve the convergence of the original SDUGKS for an optically thick system in solving the multigroup neutron Boltzmann transport equation (NBTE) to analyze the distribution of fission energy in the reactor core. In the accelerated SDUGKS, by solving the coarse mesh macroscopic governing equations (MGEs) derived from the moment equations of the NBTE, the numerical solutions of the NBTE on fine meshes at the mesoscopic level can be rapidly obtained from the prolongation of the coarse mesh solutions of the MGE. Furthermore, the use of the coarse mesh can greatly reduce the computational variables and improve the computational efficiency of the MGE. The biconjugate gradient stabilized Krylov subspace method with the modified incomplete LU preconditioner and the lower-upper symmetric-Gauss-Seidel sweeping method are implemented to solve the discrete systems of the macroscopic coarse mesh acceleration model and mesoscopic SDUGKS to further improve the numerical efficiency. Numerical solutions validate good numerical accuracy and high acceleration efficiency of the proposed accelerated SDUGKS for the complicated multiscale neutron transport problems.

DOI: 10.1103/PhysRevE.107.045304

I. INTRODUCTION

The neutron transport is generally a complicated and multiscale process to analyze the distribution of fission energy and can be described by the neutron Boltzmann transport equation (NBTE) for the distribution function or the angular flux as a function of position, transport direction, energy, and time [1,2]. Due to the seven degrees of freedom for the angular flux, it is very challenging to efficiently and accurately solve the NBTE in practical engineering applications. Up to now, a number of numerical methods, such as the Monte Carlo method [3], the spherical harmonics method (P_N) [4], the simplified P_N [5], the collision probability method [6], the method of characteristics (MOC) [7], and the discrete ordinate method (S_N or DOM) [8,9], have been developed and widely used to solve the NBTE.

The Monte Carlo method is a stochastic method that is more expensive for large-scale reactor core systems [1]. The P_N method is one of the classical methods in which the angular fluxes and the source terms are expanded in spherical harmonics and the coupled moment equations are numerically solved. However, the mathematical derivation of the P_N method is rather complicated and difficult as the expansion order of spherical harmonics increases. The collision probability method is based on the probability of a neutron from birth to its first collision in the material regions by tracking all the neutron trajectories to compute the neutron flux; this method is preferred for small-scale problems filled with a small number of materials. The MOC solves the characteristic form of the NBTE by following the neutron paths, and the scalar flux can be constructed by collecting all the average angular fluxes based on the incoming angular fluxes and the sources inside the region. The MOC has the capability to solve the complicated transport problems, but the MOC requires extensive computational costs for three-dimensional full core models [2]. The S_N or DOM has been widely used to solve various particle transport problems and nonequilibrium flows. Generally, in the traditional S_N method, the direct interpolation methods, such as the (weighted) diamond difference method and the step scheme, are used to evaluate the interface flux between the neighboring cells by only considering the free transport of the neutron and ignoring the effects of collision, scattering, and fission [1,9]. Therefore, the traditional S_N method requires a very small cell size to reduce the significant errors for the transport problems in which the collision, scattering, or absorption process happens frequently, especially for problems with thick optical thickness.

Recently, by making full use of the characteristic information of the BTE and the numerical framework of S_N, the finite-volume discrete unified gas kinetic scheme (DUGKS) [10,11] have been successfully developed for multiscale transport problems such as gas flow [12], the radiative transfer [13], phonon [14], plasma [15], and neutron transports [16,17]. In DUGKS, the transport and scattering effects in reconstructing

*Corresponding author: zhouxiafeng@hust.edu.cn
†Corresponding author: zlguo@hust.edu.cn

the interface flux are such that DUGKS has good asymptotic preserving [18] and self-adaptive multiscale properties [19,20]. Recently, the DUGKS was extended to steady NBTE in delta form (SDUGKS) [17]. However, the original MOC, S_N, and SDUGKS methods for the steady NBTE usually converge very slowly for the optically thick systems due to the frequent particle collisions [21]. To improve the convergence rate of the classical S_N method, it is noted that some acceleration methods have been proposed from different viewpoints, such as the diffusion synthetic acceleration [22,23], the transport synthetic acceleration [24], coarse mesh finite difference acceleration [25–28], coarse mesh rebalance acceleration [29,30], multigrid method [31,32], Krylov iterative method [33,34], and Jacobian-free Newton Krylov method [35]. The contribution of the acceleration methods is to update the macroscopic variables by solving the moment equations derived from the NBTE or to improve the computational efficiency based on efficient iterative methods.

In the present work, an efficient numerical method which combines the SDUGKS and the macroscopic coarse mesh acceleration is developed, which provides a potential numerical tool for the more complicated multiscale neutron transport problems with a wide range of optical thickness in the practical engineering applications. The angular fluxes, macroscopic scalar fluxes, and the source terms in the NBTE using the SDUGKS are predicted and updated from the prolongation of the coarse mesh solutions of the macroscopic governing equation derived from the moment equations of the NBTE.

The remainder of the paper is organized as follows. Section II presents the detailed theoretical analysis and the formulation of the SDUGKS with the macroscopic coarse mesh acceleration, including the formulation of the SDUGKS for the steady multigroup NBTE, the delta-form-based iterative method for SDUGKS, and the macroscopic coarse mesh acceleration technique for SDUGKS. In Sec. III, three typical neutron transport problems are solved to verify the numerical properties of the proposed accelerated SDUGKS. Finally, some conclusions are presented in Sec. IV.

II. SDUGKS WITH MACROSCOPIC COARSE MESH ACCELERATION

A. SDUGKS for steady neutron Boltzman transport equation

By integrating the NBTE on the energy interval $[E_{g-1/2},\ E_{g+1/2}]$ with $g = 1, \ldots, G$, the steady multigroup NBTE for the angular flux or the distribution function ψ as a function of position $\vec{r}$, transport direction $\vec{\Omega}$ for the k-eigenvalue problem with isotropic scattering model [1,2] can be written as

$$\vec{\Omega}\cdot\nabla\psi_g(\vec{r},\vec{\Omega}) = Q_g(\vec{r},\ \vec{\Omega}) - \Sigma_{t,g}(\vec{r})\psi_g(\vec{r},\ \vec{\Omega}), \tag{1}$$

$$Q_g(\vec{r},\ \vec{\Omega}) = q_{g,\mathrm{scatter}}(\vec{r}) + \frac{\chi_g}{k_{\mathrm{eff}}} q_{g,\mathrm{fission}}(\vec{r}), \tag{2}$$

$$\begin{aligned} q_{g,\mathrm{scatter}}(\vec{r}) &= \sum_{g'=1}^{G} \Sigma_{s,g'\to g}(\vec{r})\phi_{g'}(\vec{r}) \\ &= \Sigma_{s,\ g\to g}(\vec{r})\phi_g(\vec{r}) + S_{g,\mathrm{scatter}}(\vec{r}), \end{aligned} \tag{3}$$

$$q_{g,\mathrm{fission}}(\vec{r}) = \sum_{g'=1}^{G} \upsilon\Sigma_{f,\ g'}\phi_{g'}(\vec{r}), \tag{4}$$

$$\phi_g(\vec{r}) = \int \psi_g(\vec{r},\ \vec{\Omega})d\vec{\Omega},$$

$$S_{g,\mathrm{scatter}}(\vec{r}) = \sum_{\substack{g'=1\\ g'\neq g}}^{G} \Sigma_{s,g'\to g}(\vec{r})\phi_{g'}(\vec{r}), \tag{5}$$

where ψ_g is the gth group distribution function or angular flux. $\Sigma_{t,g}$, $\Sigma_{s,g'\to g}$, $\upsilon\Sigma_{f,\,g}(\vec{r})$, and χ_g are the group average total cross section, scattering cross section from group g' to g, fission cross section, and fission spectrum, respectively; k_{eff} is the effective multiplication factor representing the ratio of the neutrons produced in one generation to the number of neutrons lost in the preceding generation; $\phi_g(\vec{r})$ is the macroscopic scalar flux by integrating the angular flux $\psi_g(\vec{r},\ \vec{\Omega})$ over the transport direction space $\vec{\Omega}$.

The source term Q_g consists of the scattering source $q_{g,\mathrm{scatter}}$ and the fission source $q_{g,\mathrm{fission}}$, which are determined by all group angular fluxes and are coupled with each other. Furthermore, due to the strong heterogeneity and complicated material distributions for the realistic nuclear reactor problems, the steady multigroup NBTE usually involves a wide range of optical thickness.

SDUGKS adopts the S_N methods [36–38] to divide the angular space $\vec{\Omega}$ into M discretized directions, and discretize the spatial space $\vec{r}$ using the finite-volume method. The resultant discrete systems can be written as

$$\frac{1}{V_c}\sum_f (\vec{\Omega}_m\cdot\vec{n}_f)\psi_{g,m}(\vec{r}_f)\Delta S_f + \Sigma_{t,g}(\vec{r}_c)\psi_{g,m}(\vec{r}_c) = Q_{g,m}(\vec{r}_c), \tag{6}$$

$$\phi_g = \sum_{m=1}^{M} \psi_{g,m}\omega_m, \tag{7}$$

where $\psi_{g,m}$ is the averaged angular flux over the discrete angular space interval $\Delta\vec{\Omega}_m$ along the neutron transport direction $\vec{\Omega}_m = (\mu_{x,m},\ \mu_{y,m}, \mu_{z,m})$; $\vec{n}_f$ and ΔS_f are the unit normal vector and the area of the interface f of cell c, respectively; V_c is the volume of the cell c and ω_m is the corresponding quadrature weight of $\vec{\Omega}_m = (\mu_{x,m},\ \mu_{y,m}, \mu_{z,m})$ and is normalized so that $\sum_{m=1}^{M}\omega_m = 1$.

In the SDUGKS, the angular flux at cell interface, $\psi_{g,m}(\vec{r}_f)$, is calculated by integrating Eq. (6) along the neutron transport direction $\vec{\Omega}_m$ with a certain characteristic length L_f, which leads to

$$\begin{aligned} &\frac{\psi_{g,m}(\vec{r}_f) - \psi_{g,m}(\vec{r}_f - L_f\vec{\Omega}_m)}{L_f} \\ &\quad + \Sigma_{t,g}(\vec{r}_f - L_f\vec{\Omega}_m)\psi_{g,m}(\vec{r}_f - L_f\vec{\Omega}_m) = Q_{g,m}(\vec{r}_f - L_f\vec{\Omega}_m). \end{aligned} \tag{8}$$

Then Eq. (7) can be rewritten as

$$\psi_{g,m}(\vec{r}_f) = \psi^{+}_{g,m}(\vec{r}_f - L_f\vec{\Omega}_m), \tag{9}$$

where

$$\psi^{+}_{g,m}(\vec{r}) = L_f Q_{g,m}(\vec{r}) + [1 - L_f\Sigma_{t,g}(\vec{r})]\psi_{g,m}(\vec{r}). \tag{10}$$

In the above reconstruction, both the transport term and all source terms are considered such that the SDUGKS is a self-adaptive high-resolution multiscale numerical scheme, which is different from the conventional direct interpolation methods without considering the source terms.

The variable $\psi^{+}_{g,m}(\vec{r}_f - L_f\vec{\Omega}_m)$ at the starting point of the characteristic line can be calculated by the linear interpolation. Taking the interface $\vec{r}_f = \vec{r}_{f,i+1/2,j}$ between the adjacent cells $(i,\ j)$ and $(i+1,\ j)$ in the two-dimensional problems as an example, one can obtain

$$\psi_{g,m}(\vec{r}_{f,i+1/2,j}) = \psi^{+}_{g,m}(\vec{r}_{f,i+1/2,j} - L_f\vec{\Omega}_m) = \begin{cases} \psi^{+}_{g,m}(\vec{r}_{c,i,j}) + (\vec{r}_{f,i+1/2,j} - L_f\vec{\Omega}_m - \vec{r}_{c,i,j})\cdot\vec{\sigma}(\vec{r}_{c,i,j}) & \mu_{x,m} > 0 \\ \psi^{+}_{g,m}(\vec{r}_{c,i+1,j}) + (\vec{r}_{f,i+1/2,j} - L_f\vec{\Omega}_m - \vec{r}_{c,i+1,j})\cdot\vec{\sigma}(\vec{r}_{c,\ i+1,j}) & \mu_{x,m} < 0, \end{cases} \tag{11}$$

$$\vec{\sigma}(\vec{r}_{c,i,j}) = \frac{\psi_{g,m}(\vec{r}_{f,i+1/2,j}) - \psi_{g,m}(\vec{r}_{f,i-1/2,j})}{\Delta h_x}, \tag{12}$$

where Δh_r $(r = x, y)$ is the cell size in each coordinate. In this paper the slope $\vec{\sigma}$ in every cell can be approximated by the interface angular flux rather than the angular flux in the cell center so that the slope $\vec{\sigma}$ can be easily computed within the cell c rather than three adjacent cells. It is noted that other reconstruction methods of the slope in the original SDUGKS [17] and the DUGKS [11] are also available.

B. Delta-form-based iterative method for SDUGKS

In the SDUGKS, the source (power) iteration [1] is adopted to compute the effective multiplication factor k_{eff} for the steady k-eigenvalue problem in the outer iterative step from n to $n+1$:

$$\frac{1}{V_c}\sum_f(\vec{\Omega}_m\cdot\vec{n}_f)\psi^{n+1}_{g,m}(\vec{r}_f)\Delta S_f + \Sigma_{t,g}(\vec{r}_c)\psi^{n+1}_{g,m}(\vec{r}_c) = \Sigma_{s,g\to g}(\vec{r}_c)\phi^{n+1}_g(\vec{r}_c) + \sum_{\substack{g'=1\\ g'\neq g}}^{G}\Sigma_{s,g'\to g}(\vec{r}_c)\phi^{n+1}_{g'}(\vec{r}_c) + \frac{\chi_g}{k^n_{\text{eff}}}q^n_{g,\text{fission}}(\vec{r}_c), \tag{13}$$

$$k^{n+1}_{\text{eff}} = k^n_{\text{eff}}\frac{\int_V q^{n+1}_{g,\text{fission}}(\vec{r})dV}{\int_V q^n_{g,\text{fission}}(\vec{r})dV}. \tag{14}$$

In the inner iterative steps to update the gth group angular flux, based on the known scalar flux $\phi^{n+1,\ l}_g$ in the lth inner iterative step, the new value of $\psi_{g,m}$ can be obtained by

$$\frac{1}{V_c}\sum_f(\vec{\Omega}_m\cdot\vec{n}_f)\psi^{n+1,l+1}_{g,m}(\vec{r}_f)\Delta S_f + \Sigma_{t,g}(\vec{r}_c)\psi^{n+1,l+1}_{g,m}(\vec{r}_c) = \Sigma_{s,g\to g}(\vec{r}_c)\phi^{n+1,l}_g(\vec{r}_c) + S_{g,m}(\vec{r}_c), \tag{15}$$

$$S_{g,m}(\vec{r}_c) = \sum_{g'=1}^{g-1}\Sigma_{s,g'\to g}(\vec{r}_c)\phi^{n+1,l+1}_{g'}(\vec{r}_c) + \sum_{g'=g+1}^{G}\Sigma_{s,g'\to g}(\vec{r}_c)\phi^{n+1,l}_{g'}(\vec{r}_c) + \frac{\chi_g}{k^n_{\text{eff}}}q^n_{g,\text{fission}}(\vec{r}_c). \tag{16}$$

By introducing $\psi^{n+1,l+1}_{g,m} = \psi^{n+1,l}_{g,m} + \Delta\psi^{n+1,l}_{g,m}$, Eq. (15) can be written in delta form as

$$\frac{1}{V_c}\sum_f(\vec{\Omega}_m\cdot\vec{n}_f)\Delta\psi^{n+1,l}_{g,m}(\vec{r}_f)\Delta S_f + \Sigma_{t,g}(\vec{r}_c)\Delta\psi^{n+1,l}_{g,m}(\vec{r}_c) = R^{n+1,l}_{g,m}(\vec{r}_c), \tag{17}$$

$$R^{n+1,l}_{g,m}(\vec{r}_c) = \Sigma_{s,g\to g}(\vec{r}_c)\phi^{n+1,l}_g(\vec{r}_c) + S_{g,m}(\vec{r}_c) - \Sigma_{t,g}(\vec{r}_c)\psi^{n+1,l}_{g,m}(\vec{r}_c) - \frac{1}{V_c}\sum_f(\vec{\Omega}_m\cdot\vec{n}_f)\psi^{n+1,l}_{g,m}(\vec{r}_f)\Delta S_f \tag{18}$$

Actually, since the increment $\Delta\psi$ and all the terms on the left-hand side of Eq. (17) vanish when the iteration converges, the final numerical accuracy is only determined by the residual functions $R^{n+1,l}_{g,m}$. Therefore, the simple and stable step (upwind) scheme can be used to discretize the terms

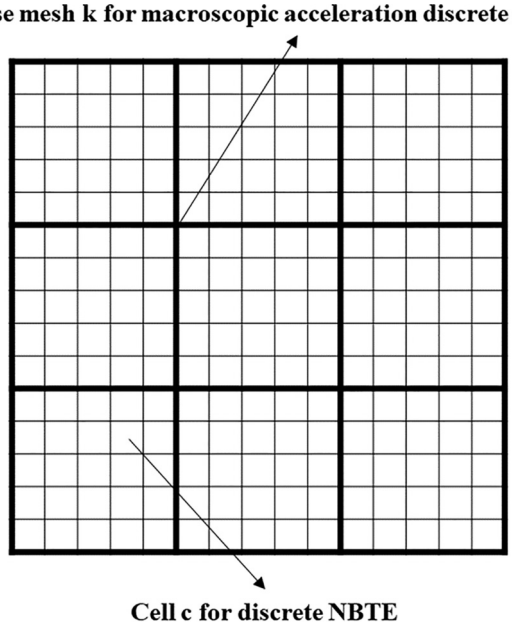

FIG. 1. Cell/mesh for the NBTE and macroscopic acceleration discrete systems.

on the left-hand side, and the SDUGKS is adopted to discretize the interface flux $\psi_{g,m}^{n+1,l}(\vec{r}_f)$ on the right-hand side to ensure high-resolution numerical results. The lower-upper symmetric-Gauss-Seidel sweeping method [17] is used to solve Eq. (17) to obtain the increment $\Delta\psi_{g,m}^{n+1,l}$. Then $\psi_{g,m}^{n+1,l+1}$ is updated until the convergence criterion is reached. The detailed analysis and iterative strategies of the SDUGKS with the delta form can be found in Ref. [17].

However, the original SDUGKS may converge very slowly for optically thick systems in the near-diffusion regime because the particle mean free path is far less than the characteristic system length and significant numbers of particles undergo many collisions before being captured or leaking out [21], which leads to rather expensive computational costs for practical engineering problems.

C. Macroscopic coarse mesh acceleration using Krylov subspace method for SDUGKS

To improve the convergence rate of the original SDUGKS for optically thick systems, the macroscopic coarse mesh acceleration technique will be introduced, which solves the macroscopic governing equations derived from the moment equations of the NBTE on a coarser mesh. Actually, the macroscopic acceleration model can be viewed as "angular multigrid" methods with the two grid levels for SDUGKS and the macroscopic coarse mesh spatial discretization is also a "spatial multigrid" method with the two grid levels. Therefore, the proposed macroscopic coarse mesh acceleration models can be viewed as the combination of "angular multigrid" and "spatial multigrid" methods. Specifically, the moments of the angular flux [22,23] are defined by

$$\phi_{g,p}^{q} = \int Y_p^q(\vec{\Omega})\psi_g(\vec{r},\ \vec{\Omega})d\vec{\Omega} = \sum_{m=1}^{M} Y_p^q(\mu_{x,m}, \varphi_m)\psi_{g,m}\omega_m, \tag{19}$$

where the spherical harmonics polynomials [22,23] are defined as

$$Y_p^q(\mu, \varphi) = \sqrt{\frac{(2-\delta_{q0})(p-q)!}{(p+q)!}} P_p^q(\mu)\cos(q\varphi), \tag{20}$$

$$\cos(\varphi) = \frac{\mu_y}{\sqrt{1-(\mu_x)^2}}, \tag{21}$$

$$P_0^0(x) = 1, \quad P_1^0(x) = x, \quad \text{and} \quad P_1^1(1-x^2)^{1/2}. \tag{22}$$

The functions P_p^q are the associated Legendre polynomials. It is obvious that $\phi_{g,0}^0 = \phi_g$. Taking the two-dimensional

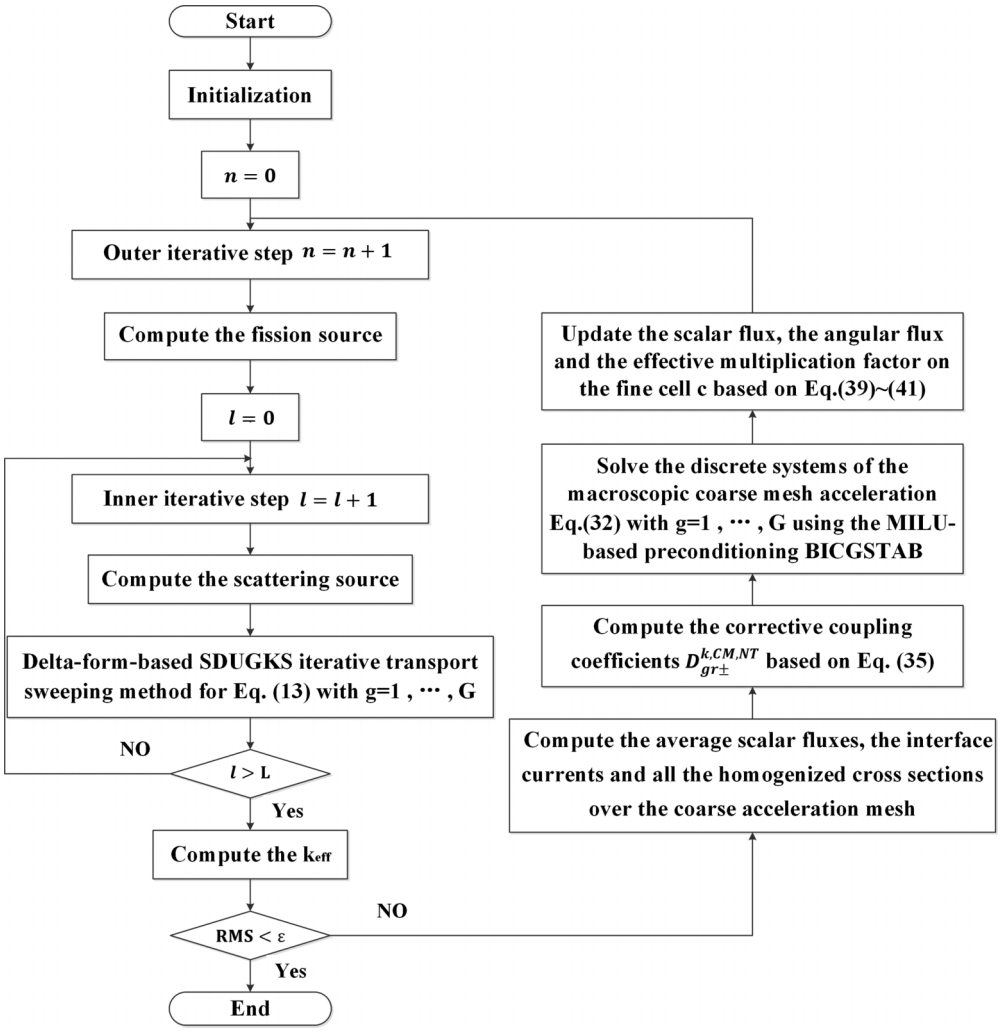

FIG. 2. Algorithm and flowchart of the accelerated SDUGKS.

TABLE I. Cross sections of the two-dimensional homogeneous bare square reactor.

Case	Σ_t	Σ_a	Σ_s	ε	$\Sigma_t h$
A	$1/\varepsilon$	0.1ε	$1/\varepsilon - 0.1\varepsilon$	0.01	10
B				0.001	100
C				0.0001	1000
D	$\frac{1}{\varepsilon}[1+50(x^2+y^2)]$, $x \in [0,1]$, $y \in [0,1]$	0.00	$\frac{1}{\varepsilon}[1+50(x^2+y^2)]$, $x \in [0,1]$, $y \in [0,1]$	0.01	10–1000

problems as an example, the moment equations (P_1 forms) [22] can be obtained by Eqs. (23)–(25) from Eq. (1),

$$\frac{\partial \phi^0_{g,1}}{\partial x} + \frac{\partial \phi^1_{g,1}}{\partial y} + \Sigma_{t,g}\phi_g = \Sigma_{s,g\to g}\phi_g + S_{g,\text{scatter}} + q_{g,\text{fission}}, \tag{23}$$

$$\frac{1}{3}\frac{\partial \phi_g}{\partial x} + \frac{2}{3}\frac{\partial \phi^0_{g,2}}{\partial x} + \frac{\sqrt{3}}{3}\frac{\partial \phi^1_{g,2}}{\partial y} + \Sigma_{t,g}\phi^0_{g,1} = 0, \tag{24}$$

$$\frac{\sqrt{3}}{3}\frac{\partial \phi^1_{g,2}}{\partial x} + \frac{1}{3}\frac{\partial \phi_g}{\partial y} - \frac{1}{3}\frac{\partial \phi^0_{g,2}}{\partial y} + \frac{\sqrt{3}}{3}\frac{\partial \phi^2_{g,2}}{\partial y} + \Sigma_{t,g}\phi^1_{g,1} = 0, \tag{25}$$

which can be rewritten as

$$\frac{\partial \phi^0_{g,1}}{\partial x} + \frac{\partial \phi^1_{g,1}}{\partial y} + \Sigma_{R,g}\phi_g = S_{g,\text{scatter}} + q_{g,\text{fission}}, \tag{26}$$

$$\phi^0_{g,1} = J_x + O_x, \tag{27}$$

$$\phi^1_{g,1} = J_y + O_y, \tag{28}$$

$$J_r = -D_g\frac{\partial \phi_g}{\partial r} \quad \text{with } r = x, y, \tag{29}$$

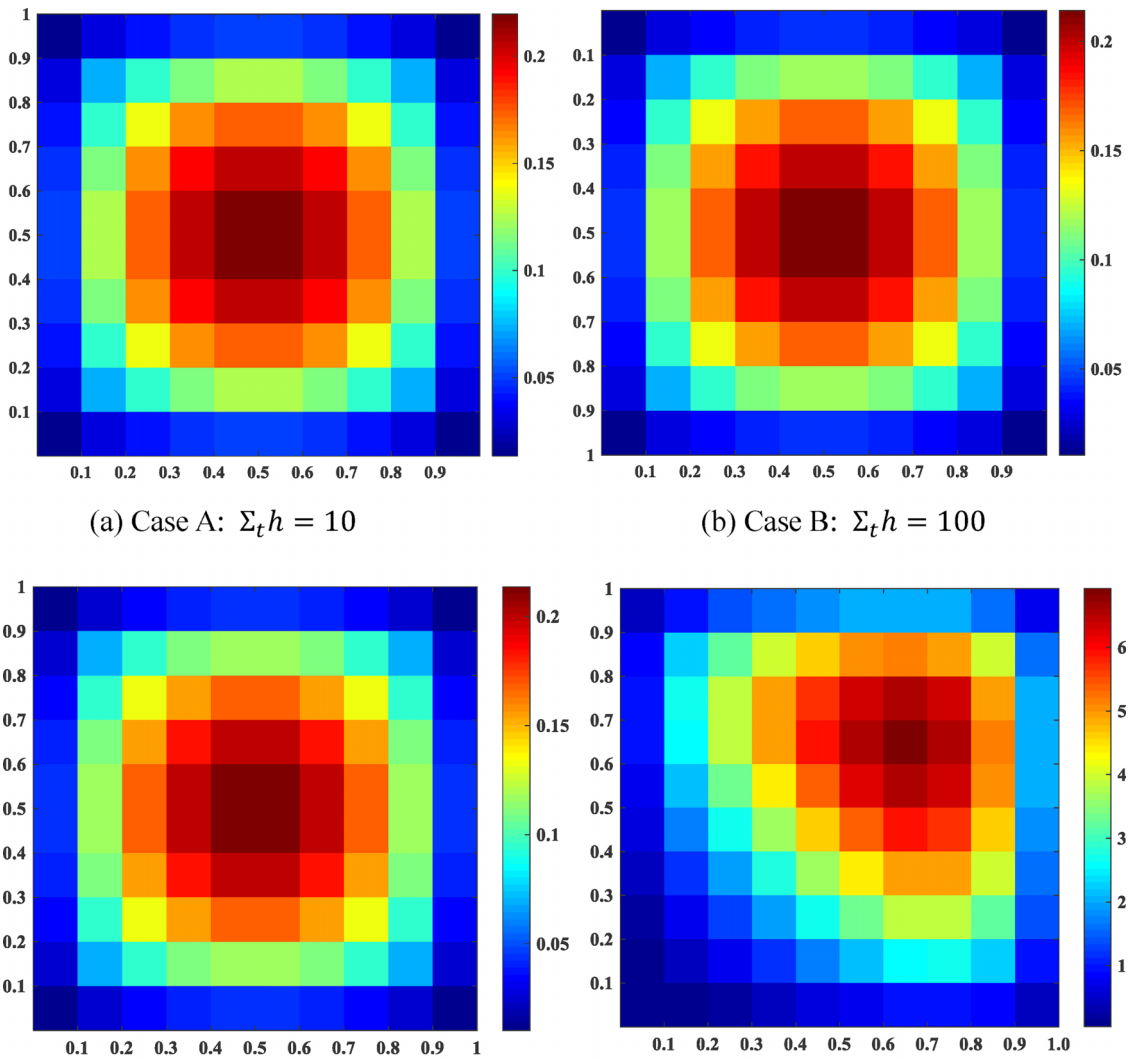

(a) Case A: $\Sigma_t h = 10$ (b) Case B: $\Sigma_t h = 100$

(c) Case C: $\Sigma_t h = 1000$ (d) Case D: $\Sigma_t h = 10\sim1000$

FIG. 3. Scalar fluxes for the four cases using the SDUGKS (cell size: 0.1×0.1).

$$O_x = -\frac{1}{3\Sigma_{t,g}}\left(2\frac{\partial\phi^0_{g,2}}{\partial x} + \sqrt{3}\frac{\partial\phi^1_{g,2}}{\partial y}\right), \tag{30}$$

$$O_y = -\frac{1}{3\Sigma_{t,g}}\left(\sqrt{3}\frac{\partial\phi^1_{g,2}}{\partial x} - \frac{\partial\phi^0_{g,2}}{\partial y} + \sqrt{3}\frac{\partial\phi^2_{g,2}}{\partial y}\right), \tag{31}$$

where $\Sigma_{R,g} = \Sigma_{t,g} - \Sigma_{s,g\to g}$ is the removal cross section d and $D_g = 1/3/\Sigma_{t,g}$ is the diffusion coefficient. It can be seen that $\phi^0_{g,1}$ and $\phi^1_{g,1}$ are the net currents in the x and y directions, respectively.

In the diffusion limit, O_x and O_y can be neglected since the second-order moments can be ignored [22,23]. Therefore, the net currents $\phi^0_{g,1} = J_x$ and $\phi^1_{g,1} = J_y$, respectively, which satisfy the Fick's law. However, it can be observed from Eqs. (27)–(29) that some differences exist generally between the net currents $\phi^0_{g,1}$ and $\phi^1_{g,1}$ from the NBTE and the currents J_x and J_y from the diffusion equations. Therefore, in this study the net currents $\phi^0_{g,1}$ and $\phi^1_{g,1}$ from the NBTE are calculated by both finite difference (FD) approximation of the currents J_x and J_y in Eq. (29) and additional correction terms [28] to ensure the equivalence between net currents $\phi^0_{g,1}$ and $\phi^1_{g,1}$ and the currents J_x and J_y. At the same time, the macroscopic equation (26) can be discretized with a coarser mesh than the same one used for the discretization of NBTE due to the above-mentioned correction terms [27,28,39]. The discrete form of Eq. (26) can be written as

$$\frac{\phi^{0,k,\mathrm{CM}}_{g,1,x+} - \phi^{0,k,\mathrm{CM}}_{g,1,x-}}{\Delta h^{k,\mathrm{CM}}_x} + \frac{\phi^{1,k,\mathrm{CM}}_{g,1,y+} - \phi^{1,k,\mathrm{CM}}_{g,1,y-}}{\Delta h^{k,\mathrm{CM}}_y} + \Sigma^k_{R,g,\mathrm{CM}}\phi^k_{g,\mathrm{CM}} = S^k_{g,\mathrm{scatter,CM}} + q^k_{g,\mathrm{fission,CM}}, \tag{32}$$

where

$$\phi^{0,k,\mathrm{CM}}_{g,1,x\pm} \text{ or } \phi^{1,k,\mathrm{CM}}_{g,1,y\pm} = \mp D^{k,\mathrm{CM,FD}}_{gr\pm}\left(\phi^{k\pm1}_{g,\mathrm{CM}} - \phi^k_{g,\mathrm{CM}}\right) - D^{k,\mathrm{CM,NT}}_{gr\pm}\left(\phi^{k\pm1}_{g,\mathrm{CM}} + \phi^k_{g,\mathrm{CM}}\right). \tag{33}$$

The subscript $r\pm$ $(r = x, y)$ denotes the two net currents at $r = \pm\Delta h^{k,\mathrm{CM}}_r/2$ for the coarse acceleration mesh k with $k = 1, \ldots, K$. The superscript CM denotes the variables defined on the coarse acceleration mesh as shown in Fig. 1.

The FD diffusion coefficients $D^{k,\mathrm{CM,FD}}_{gr\pm}$ on the coarse acceleration mesh are calculated by the harmonic average of $D^{k\pm1,\mathrm{CM}}_{gr}$ and $D^{k,\mathrm{CM}}_{gr}$ over the two adjacent coarse acceleration

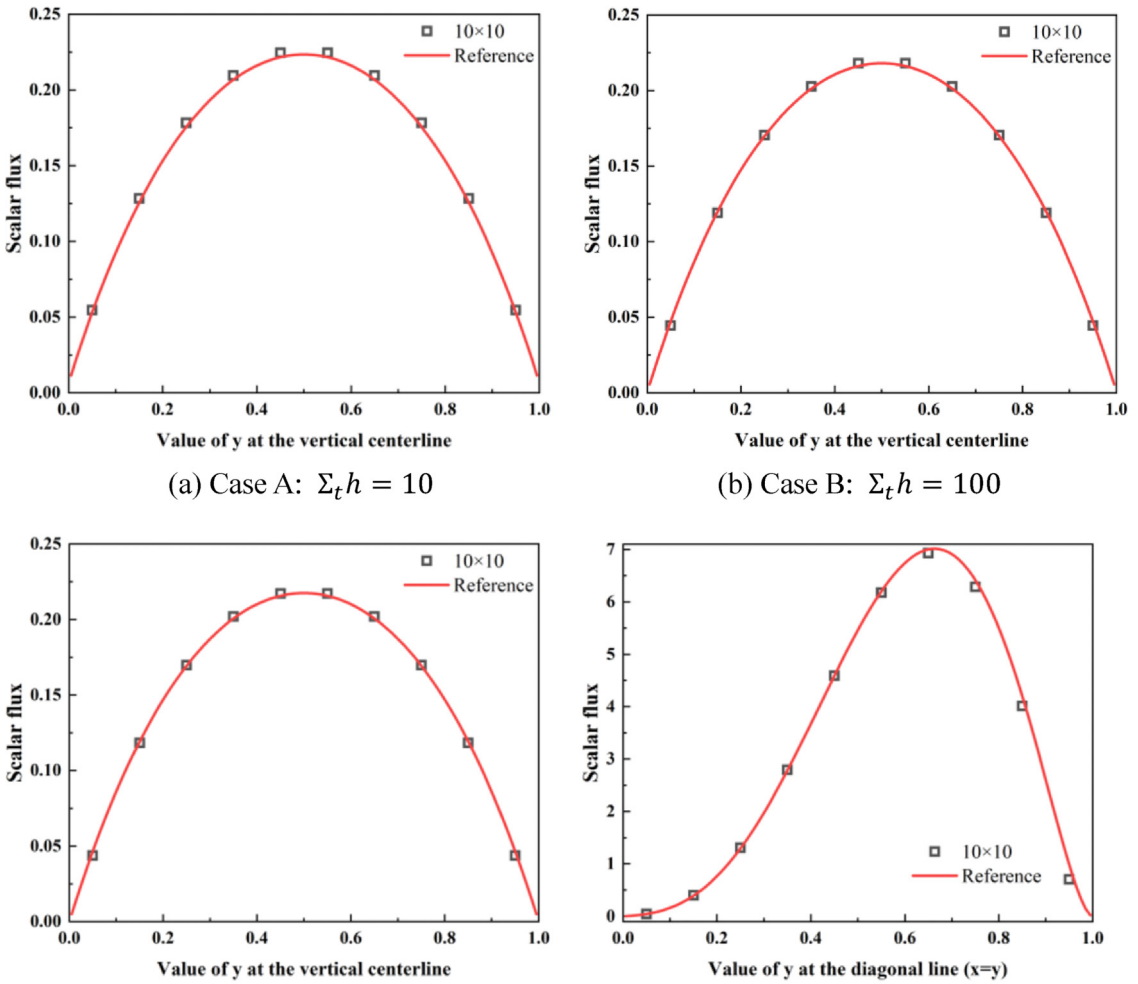

(a) Case A: $\Sigma_t h = 10$ (b) Case B: $\Sigma_t h = 100$

(c) Case C: $\Sigma_t h = 1000$ (d) Case D: $\Sigma_t h = 10\sim1000$

FIG. 4. Profile of scalar fluxes for cases A–D with the different optical thickness.

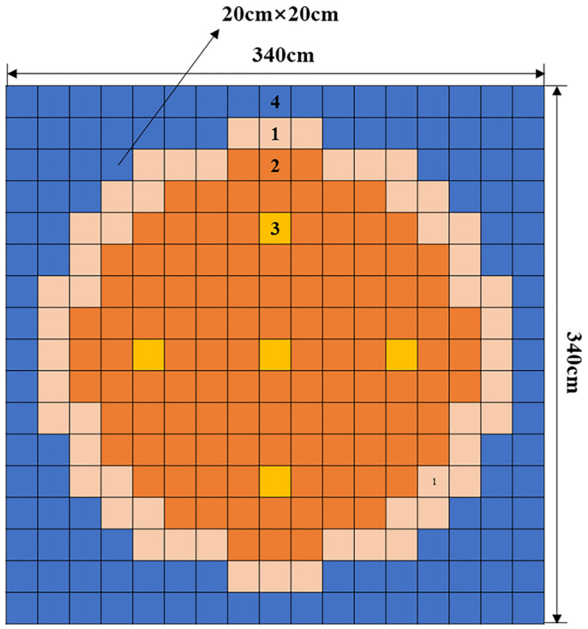

FIG. 5. Configuration of modified IAEA full core problems.

meshes:

$$D_{gr\pm}^{k,\mathrm{CM,FD}} = \frac{2D_g^{k\pm1,\mathrm{CM}} D_g^{k,\mathrm{CM}}}{D_g^{k\pm1,\mathrm{CM}} \Delta_r^{k,\mathrm{CM}} + D_g^{k,\mathrm{CM}} \Delta_r^{k\pm1,\mathrm{CM}}}. \tag{34}$$

The second term (the correction part) on the right-hand side of Eq. (33) is introduced to ensure the consistency between the interfacial net currents from the macroscopic coarse mesh acceleration calculation and those from the NBTE. The coupling coefficients $D_{gr\pm}^{\mathrm{CM,NT}}$ can be calculated by

$$D_{gr\pm}^{k,\mathrm{CM,NT}} = -\frac{J_{gr\pm}^{k,\mathrm{CM,NT}} \pm D_{gr\pm}^{k,\mathrm{CM,FD}} \left(\phi_{g,\mathrm{CM}}^{k\pm1,\mathrm{NT}} - \phi_{g,\mathrm{CM}}^{k,\mathrm{NT}}\right)}{\left(\phi_{g,\mathrm{CM}}^{k\pm1,\mathrm{NT}} + \phi_{g,\mathrm{CM}}^{k,\mathrm{NT}}\right)}, \tag{35}$$

where the currents $J_{gr\pm}^{k,\mathrm{CM,NT}}$ and $\phi_{g,\mathrm{CM}}^{k}$ on the coarse acceleration mesh can be estimated by averaging the angular flux from the NBTE on the fine cell within the coarse acceleration mesh,

$$\phi_{g,\mathrm{CM}}^{k,\mathrm{NT}} = \frac{\sum_{c\in k} \omega_m \psi_{g,m}^{n+1,L}(\vec{r}_c) V_c}{\sum_{c\in k} V_c}, \tag{36}$$

$$J_{gr\pm}^{k,\mathrm{CM,NT}} = \sum_{f\in f_{\mathrm{CM}}} \omega_m \mu_{rm} \psi_{g,m}^{n+1,L}(\vec{r}_f), \tag{37}$$

where f_{CM} is the interface between the two adjacent coarse acceleration meshes, and the overall homogenized cross section over the coarse acceleration mesh can be obtained by applying the flux-volume weighted homogenization,

$$\Sigma_{[t,s,f],g,\mathrm{CM}}^{k} = \frac{\sum_{c\in k} \Sigma_{[t,s,f],g}(\vec{r}_c) \psi_{g,m}^{n+1,L}(\vec{r}_c) V_c}{\sum_{c\in k} \psi_{g,m}^{n+1,L}(\vec{r}_c) V_c}. \tag{38}$$

Based on Eqs. (33)–(38), the discrete system of the macroscopic coarse mesh acceleration Eq. (32) exhibits a five-point [for two-dimensional (2D) models] or seven-point (for three-dimensional models) stencils, which leads to a five-diagonal or seven-diagonal $K\times K$ sparse matrix for every group. The biconjugate gradient stabilized Krylov subspace method with the modified incomplete LU preconditioner [40,41] is adopted to solve the discrete system.

Once the macroscopic scalar fluxes $\phi_{g,\mathrm{CM}}^{k}$ and the effective multiplication factor $k_{\mathrm{eff,CM}}$ are obtained, they can be used to update the scalar flux, angular flux, and the effective multiplication factor k_{eff} on the fine mesh:

$$\phi_g^{n+1,L}(\vec{r}_c) = \phi_g^{n+1,L}(\vec{r}_c) \frac{\phi_{g,\mathrm{CM}}^{k}}{\phi_{g,\mathrm{CM}}^{k,\mathrm{NT}}}, \tag{39}$$

$$\psi_{g,m}^{n+1,L}(\vec{r}_c) = \psi_{g,m}^{n+1,L}(\vec{r}_c) + \frac{4\left(\phi_{g,\mathrm{CM}}^{k} - \phi_{g,\mathrm{CM}}^{k,\mathrm{NT}}\right)}{\omega_m M}, \tag{40}$$

$$k_{\mathrm{eff}}^{n+1} = k_{\mathrm{eff,CM}}. \tag{41}$$

And then the inner iteration in Eqs. (15) and (16) can be continued in the next iterative step to update the g-th group angular flux.

D. Algorithm and acceleration strategy

The algorithm and flowchart of the accelerated SDUGKS are presented in Fig. 2. The overall procedure contains outer and inner iterations. At each outer iteration step n, the effective multiplication factor k_{eff} and fission source $q_{g,\mathrm{fission}}$ are calculated using the power iteration method, and at each inner iterative step l per the outer iteration, the neutron flux and scattering source $q_{g,\mathrm{scatter}}$ are updated. The macroscopic coarse mesh acceleration iteration is implemented after every outer iteration n.

TABLE II. Cross section of modified IAEA full core system (cm^{-1}).

Region	Material	Group	$\Sigma_{t,g}$	$\Sigma_{a,g}$	$\nu\Sigma_{f,g}$	$\Sigma_{s,g\to g}$	$\Sigma_{s,g\to g+1}$
1	Fuel 1	1	0.222222	0.010120	0.000000	0.192102	0.020000
		2	0.833333	0.080032	0.135000	0.753301	
2	Fuel 2	1	0.222222	0.010120	0.000000	0.192102	0.020000
		2	0.833333	0.085032	0.135000	0.748301	
3	Fuel 2+rod	1	0.222222	0.010120	0.000000	0.192102	0.020000
		2	0.833333	0.130032	0.135000	0.703301	
4	Reflector	1	0.166667	0.000160	0.000000	0.126507	0.040000
		2	1.111111	0.010024	0.000000	1.101087	

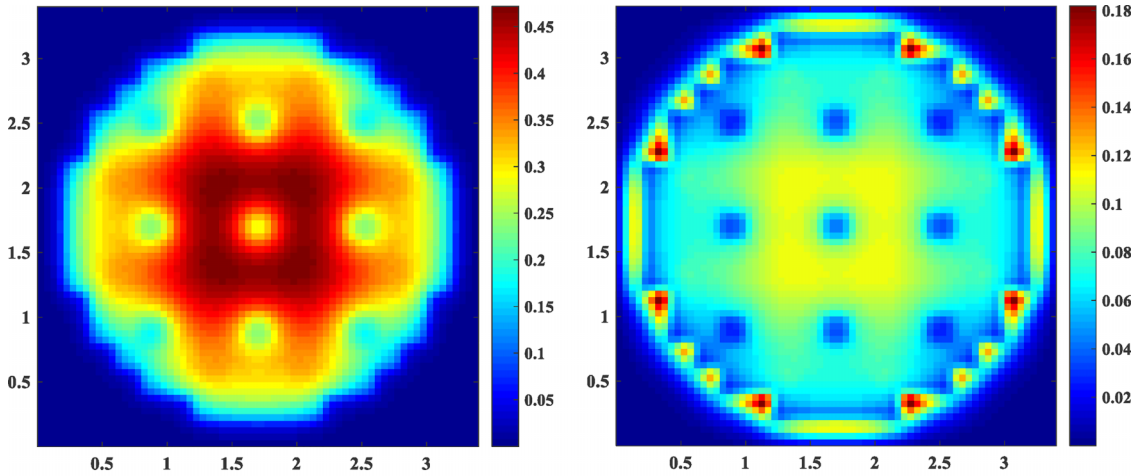

FIG. 6. Scalar flux for the two-dimensional modified IAEA full core problems using the accelerated SDUGKS (cell size: 5 cm×5 cm).

The convergence criterion is controlled by the root mean square (RMS),

$$\mathrm{RMS} = \sqrt{\frac{\sum_{c=1}^{C} \left|\phi_g^{n+1}(\vec{r}_c) - \phi_g^{n}(\vec{r}_c)\right|^2 + \left(k_{\mathrm{eff}}^{n+1} - k_{\mathrm{eff}}^{n}\right)^2}{\boldsymbol{C}+1}} < \varepsilon. \tag{42}$$

In addition, in our practical code development, the average diffusion coefficient in each coordinate on the coarse acceleration mesh is calculated as

$$D_{gr}^{k,\mathrm{CM}} = \frac{1}{3\Sigma_{t,g,\mathrm{CM}}^{k}} + 0.125\Delta h_r^{k,\mathrm{CM}} \quad \text{with } r = x, y, \tag{43}$$

where the second term on the right-hand side is used to stabilize the macroscopic iteration [28]. In addition, the macroscopic coarse mesh acceleration models only accelerate the convergence rate of SDUGKS for the NBTE by rapidly obtaining the macroscopic parameters of the NBTE and have no influence on the accuracy of SDUGKS, which can be viewed as the "predictor or preconditioner" of SDUGKS. Therefore, a loose convergence condition is generally needed for the macroscopic coarse mesh acceleration and the numerical accuracy is only determined by SDUGKS. The detailed analysis of the numerical stability can be also found in Refs. [21,28].

III. NUMERICAL RESULTS

In this section the three representative neutron transport problems are considered to test the numerical performance of the proposed accelerated SDUGKS. First, the two-dimensional one-group fixed-source problem in the diffusion limit with the different optical thicknesses [18,19] is simulated

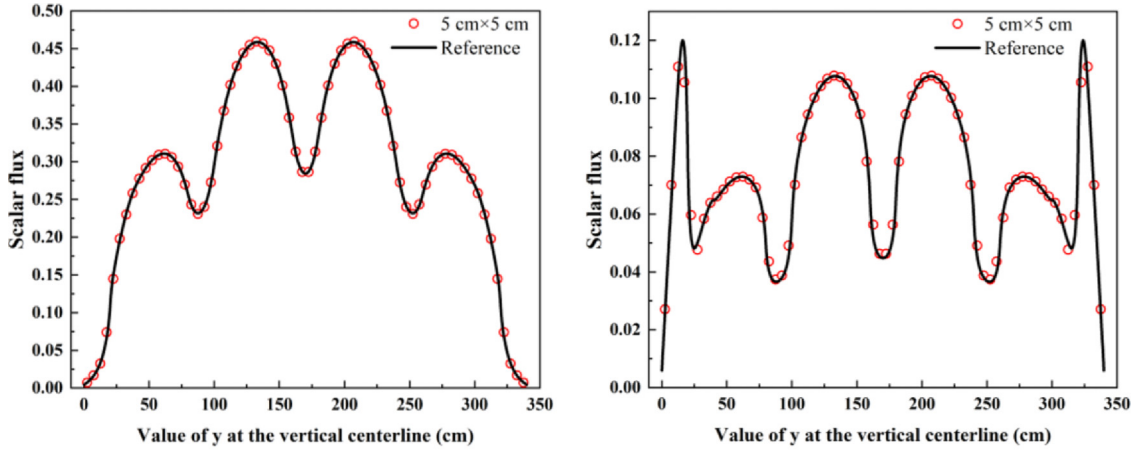

FIG. 7. Scalar fluxes at the vertical centerline for the two-dimensional modified IAEA full core system predicted by the accelerated SDUGKS.

TABLE III. Effective multiplication factor for the two-dimensional modified IAEA full core problems using the accelerated SDUGKS.

Mesh size of SDUGKS	Effective multiplication factor	Relative error
5 cm×5 cm	1.029981	0.0000981
2.5 cm×2.5 cm	1.030056	0.0000252
1.25 cm×1.25 cm	1.030075	0.0000068
Reference	1.030082	

to validate the asymptotic preserving property and multiscale performance. Then the two-dimensional modified IAEA (International Atomic Energy Agency) full core problem is simulated to further analyze the numerical accuracy and acceleration rate of the proposed method for realistic cases [42,43]. Finally, the high-resolution full core UO2-fueled assemblies/mixed oxide (UOX/MOX) pin-by-pin (at the level of fuel pin by fuel pin) transport model [44,45] with strong heterogeneity and complicated material distributions is employed to test the numerical capability and potential of the accelerated SDUGKS in simulating the large-scale practical engineering problems. In our simulations, $\varepsilon = 10^{-6}$ is chosen as the convergence criterion of the SDUGKS and the S_{12} Carlson quadrature set is adopted to discretize the angular space.

A. Test of asymptotic preserving and multiscale property

The asymptotic preserving property of a numerical scheme is important to solve the multiscale neutron transport ranging from optically thin to optically thick regimes. The asymptotic preserving schemes can give reasonable solutions to the transport problems in the diffusion limit even when the mesh size is much more than the mean free path of particles. To test the asymptotic preserving property of the proposed SDUGKS, we consider a two-dimensional homogeneous and bare square reactor of length $L = 1$ with vacuum boundary on all sides.

To test the asymptotic preserving and multiscale property of the proposed SDUGK method, four different cases are defined by changing the values of the cross-section constants as shown in Table I. The transports of cases A–C are in near-diffusion regime, while the transport of case D is a multiscale one. It is noted that the fission source term $\frac{\chi_g}{k_{\text{eff}}} q_{g,\text{fission}}(\vec{r})$ in Eq. (2) is set to ε in all cases.

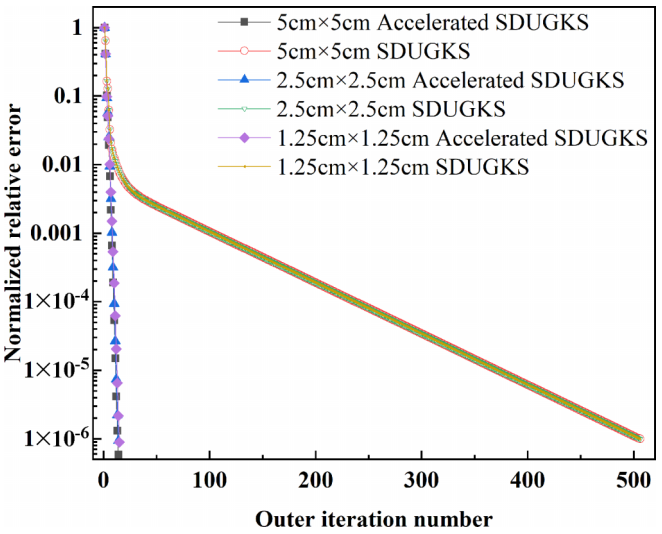

FIG. 8. Convergence rates of the original SDUGKS and accelerated SDUGKS for the two-dimensional modified IAEA full core system.

A uniform mesh with cell size with $\Delta x = \Delta y = h = 0.1$ is employed in the simulation, meaning that the ratio of cell size to mean free path, $\Sigma_t h$, ranges from 10 to 1000 in the test cases.

The predicted scalar flux fields for the four cases are presented in Fig. 3 and the profiles of the scalar flux along the vertical centerline of the reactor core are shown in Fig. 4. For all cases, the reference solutions are obtained using the S_N method with the diamond difference method on a sufficient fine mesh f size 0.01×0.01. It can be observed that the results of the present SDUGKS can agree well with the reference solutions as $\Sigma_t h$ ranges from 10 to 1000 even on the coarse mesh, which shows that the proposed SDUGKS can capture the asymptotic diffusion transport with $\Delta x = \Delta y = \varepsilon^l h$ with $l = 0$ [18], indicating the potential for simulating multiscale transport problems with a wide range of optical thicknesses.

B. Two-dimensional modified IAEA full core system

The second case is a two-group square full reactor core system by filling the external ragged regions of the popular IAEA 2D full core models [43] with the reflector material. The schematic is depicted in Fig. 5 and all the physical boundaries are vacuum. Four types of materials are arranged in the

TABLE IV. Acceleration analysis of the accelerated SDUGKS for the two-dimensional modified IAEA full core system.

	Accelerated SDUGKS						
	SDUGKS		Time (s)			Speed up	
Mesh size of SDUGKS	Time (s)	Steps	SDUGKS	Macroscopic coarse mesh	Steps	Time	Steps
5 cm×5 cm	1142.982	506	30.1804	28.2472	14	19.56	36.14
2.5 cm×2.5 cm	4549.453	506	119.1708	16.1410	14	33.62	36.14
1.25 cm×1.25 cm	17302.86	506	507.5058	25.1188	15	32.49	33.73

TABLE V. Sensitivity of the convergence criterion of the macroscopic coarse mesh acceleration for the two-dimensional modified IAEA full core system.

		Time (s)			
Convergence criterion	Mesh size	SDUGKS	Macroscopic coarse mesh	Total	Steps
0.1	5 cm×5 cm	79.7690	9.3884	89.1574	37
	2.5 cm×2.5 cm	154.0427	8.1233	162.1660	18
	1.25 cm×1.25 cm	610.3279	16.7791	627.1070	18
0.05	5 cm×5 cm	63.3286	11.6040	74.9326	29
	2.5 cm×2.5 cm	135.7677	8.9263	144.6940	16
	1.25 cm×1.25 cm	572.4194	17.6141	590.0335	17
0.01	5 cm×5 cm	30.2011	16.7852	46.9863	14
	2.5 cm×2.5 cm	127.0798	11.5130	138.5928	15
	1.25 cm×1.25 cm	539.1010	19.9851	559.0861	16
0.001	5 cm×5 cm	30.1804	28.2472	58.4276	14
	2.5 cm×2.5 cm	119.1708	16.1410	135.3118	14
	1.25 cm×1.25 cm	507.5058	25.1188	532.6246	15
0.0001	5 cm×5 cm	29.9593	36.7824	66.7417	14
	2.5 cm×2.5 cm	119.6978	24.5944	144.2922	14
	1.25 cm×1.25 cm	505.9805	31.5267	537.5072	15

modified IAEA full core regions and the two-group cross sections are listed in Table II.

In our simulations, the cell size of the coarse mesh for the macroscopic coarse mesh acceleration is 5 cm×5 cm, while three different meshes with sizes of 5 cm×5 cm, 2.5 cm × 2.5 cm, and 1.25 cm×1.25 cm are respectively adopted for the SDUGKS. The numerical solutions of the scalar fluxes predicted by the accelerated SDUGKS with the mesh of cell size 5 cm×5 cm are shown in Fig. 6. It can be seen that the scalar fluxes change dramatically in the vicinity of both the region 3 (the fuel 2 materials with control rod inserted) and the interfaces between the fuel regions (regions 1–3) and reflector (region 4). For comparison, the profiles of the fast ($g = 1$) and thermal ($g = 2$) group scalar fluxes along the vertical centerline are shown in Fig. 7, and the effective multiplication factors and relative errors are given in Table III. The reference solutions are obtained using the S_N method with the diamond difference method on a fine mesh of size 0.25 cm×0.25 cm, which is sufficient to give grid-independent results. It can be observed from Fig. 7 and Table III that the accelerated SDUGKS can still capture the transport behavior well on the coarse mesh (5 cm×5 cm), and the relative error of the effective multiplication factor is only 0.009 81%. The results further confirm the good capability of the proposed accelerated SDUGKS for the reactor neutron transport problems.

To analyze the acceleration efficiency of the accelerated SDUGKS, the convergence processes using different meshes are presented in Fig. 8, and the corresponding computation times are given in Table IV. It can be observed that the outer iterative steps of the SDUGKS is reduced from 506 to 14 or 15 steps by the macroscopic coarse mesh acceleration, and the speedup reaches 36.14 or 33.73. Particularly, for the two meshes of sizes 2.5 cm×2.5 cm and 1.25 cm×1.25 cm, the speedups in computational times and iteration steps are nearly

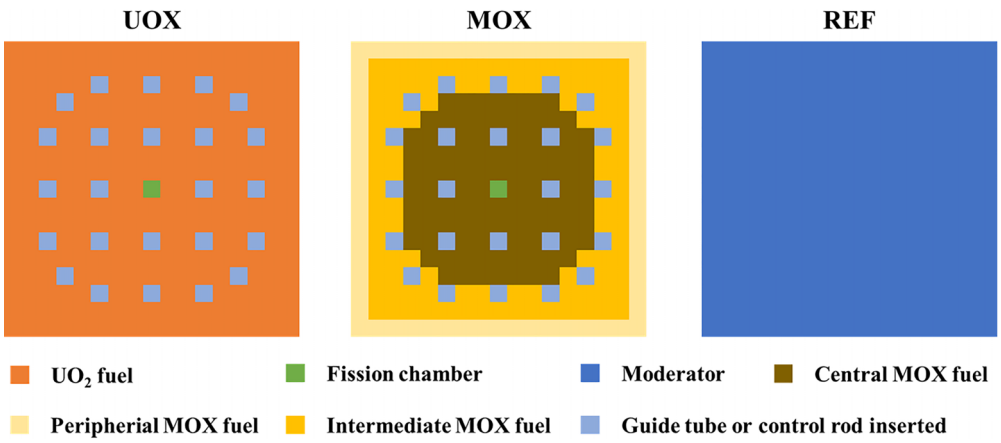

FIG. 9. Schematics of UOX, MOX and REF assembly.

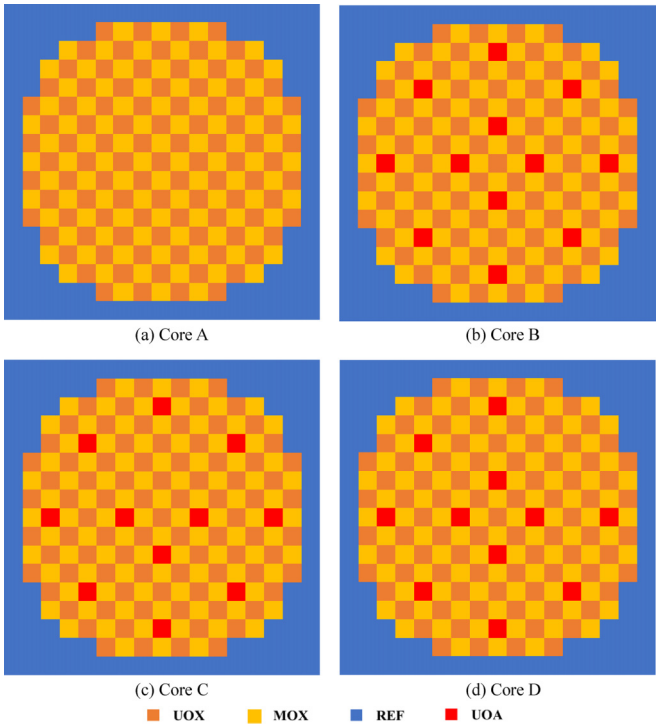

FIG. 10. Configuration of four cases of the full core UOX/MOX pin-by-pin system.

identical. This can be explained that the CPU time of the macroscopic coarse mesh acceleration is far less than that of the SDUGKS on the fine meshes. However, the speedup in CPU time is only 19.56 with the mesh of size 5 cm×5 cm, since the CPU time of the macroscopic coarse mesh

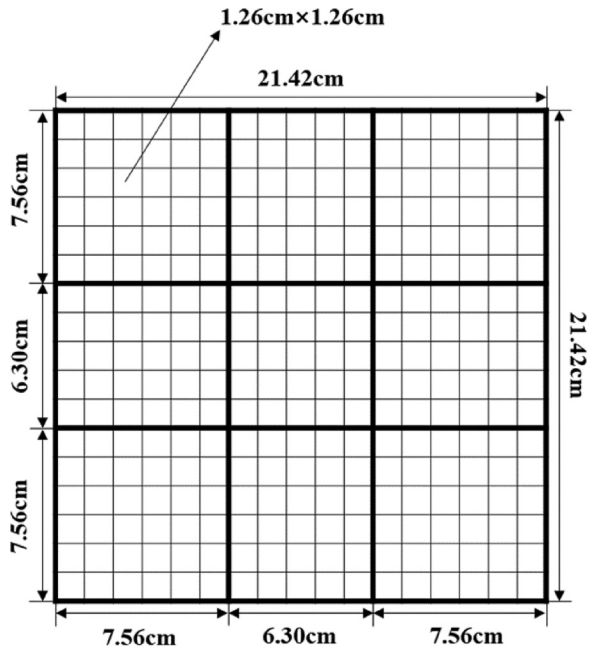

FIG. 11. Schematic of mesh generation per assembly for the SDUGKS and the macroscopic coarse mesh acceleration model.

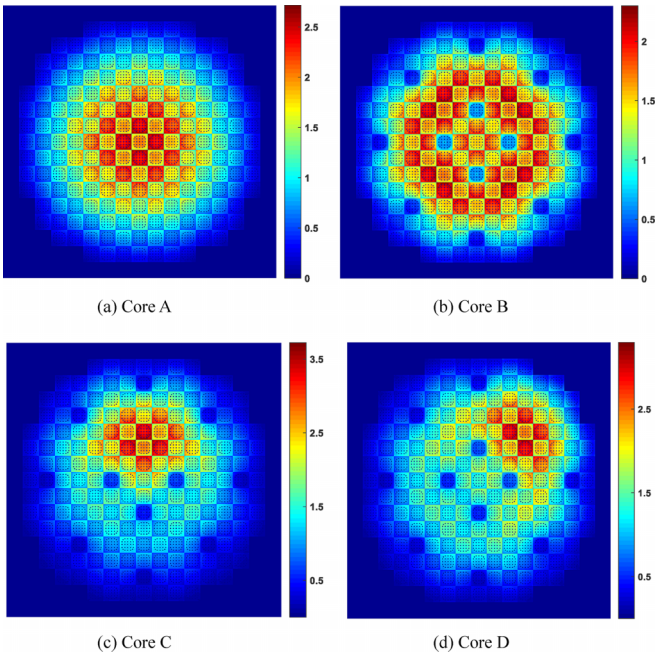

FIG. 12. Pin-by-pin power density for four cases by the accelerated SDUGKS (cell size: 1.26 cm×1.26 cm).

acceleration is nearly the same as or even more than that of the SDUGKS on the same mesh.

In addition, the sensitivity analysis of the convergence criterion of the macroscopic coarse mesh acceleration is presented in Table V. It can be seen that a loose convergence condition for the macroscopic coarse mesh acceleration will increase the iterative steps of the SDUGKS. On the other hand, a strict convergence criterion will increase the

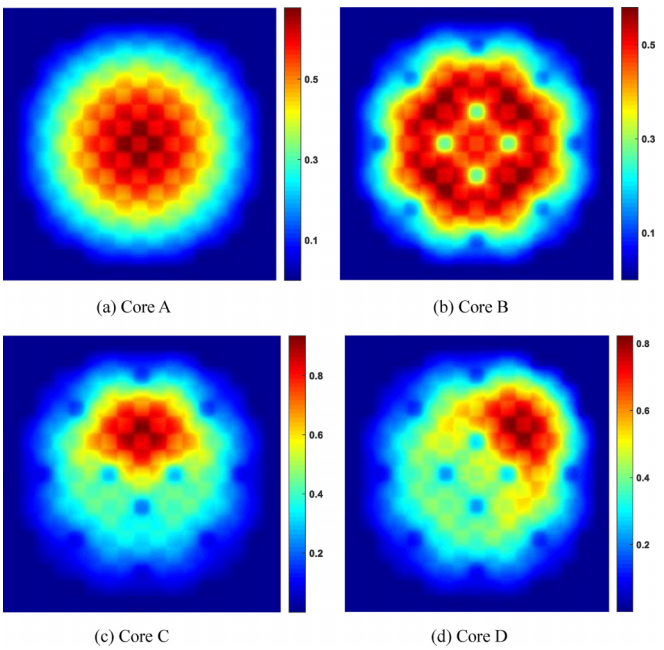

FIG. 13. Pin-by-pin fast-group scalar flux for four cases by the accelerated SDUGKS (cell size: 1.26 cm×1.26 cm).

TABLE VI. Values of cross sections of the full core UOX/MOX pin-by-pin system (cm^{-1}).

ID	Cell type	g	$\Sigma_{t,g}$	$\Sigma_{a,g}$	$\nu\Sigma_{f,g}$	$\Sigma_{s,g\to g}$	$\Sigma_{s,g\to g+1}$
1	UOX fuel	1	0.277778	0.010	0.0050	0.247778	0.020
		2	0.833333	0.100	0.1250	0	0.733333
2	Peripheral MOX fuel	1	0.277778	0.015	0.0075	0.247778	0.015
		2	0.833333	0.200	0.3000	0	0.633333
3	Intermediate MOX fuel	1	0.277778	0.015	0.0075	0.247778	0.015
		2	0.833333	0.250	0.3750	0	0.583333
4	Central MOX fuel	1	0.277778	0.015	0.0075	0.247778	0.015
		2	0.833333	0.300	0.4500	0	0.533333
5	Guide tube	1	0.277778	0.001	0	0.251778	0.025
		2	0.833333	0.020	0	0	0.813333
6	Moderator	1	0.277778	0.001	0	0.226778	0.050
		2	1.666667	0.040	0	0	1.626667
7	Fission chamber	1	0.277778	0.001	1×10^{-7}	0.251778	0.025
		2	0.833333	0.020	3×10^{-6}	0	0.813333
9	Absorber	1	0.277778	0.040	0	0.227778	0.01
		2	0.833333	0.800	0	0	0.033333

computational cost of the macroscopic coarse mesh acceleration. Generally, the convergence criterion with the value of 0.01–0.0001 can be chosen for the macroscopic coarse mesh acceleration.

C. Full core UOX/MOX pin-by-pin system

The full core UOX/MOX pin-by-pin system is a complicated full reactor core filled with 193 fuel assemblies including the traditional UO2-fueled assemblies (UOX) and weapons-grade mixed-oxide fuel assemblies (MOX) surrounded by the series of reflector assemblies (REF). Both the UOX and MOX assemblies follow a 17×17 lattice of 21.42 cm width with a 1.26-cm pitch, include 264 fuel pins, a 24-guide tube or control rod inserted, and one instrument tube for fission chamber, as shown in Fig. 9. Therefore, the whole reactor core contains 50 952 fuel pins, 4632 guide tubes or control rods, and 193 instrument tubes, which are derived from the realistic reactor geometry and data.

Four different cases are designed by the checkerboard configuration of the MOX assemblies and the UOX assemblies as depicted in Fig. 10. The red box that is defined as the UOA (UOX assembly with control rod inserted) assembly denotes the pin-by-pin UOX assembly with a control rod inserted. The different locations of the UOA assemblies are arranged for the four different cases based on different control rod behaviors and realistic reactor core operational conditions. The values of the two-group cross sections for all materials are taken from the pin-power benchmark C5 problem NEACRP-L336 [46] and are presented in Table VI, and vacuum boundary conditions are applied to all the physical boundaries.

In our simulations, a uniform mesh with cell size 1.26 cm×1.26 cm (one node per pin cell or 17×17 nodes per assembly) is used for the SDUGKS and a coarse mesh with cell size 7.56, 6.30, 7.56 cm per assembly is used for the macroscopic coarse mesh acceleration. The schematic of the mesh per assembly is shown in Fig. 11.

Figures 12 and 13 show the numerical solutions of the fast-group scalar fluxes and the pin-by-pin power densities for the four cases. It can been seen that both the fast-group scalar fluxes and the in power densities the MOX assemblies are generally greater than those in the UOX assemblies, and rapid changes can be observed in the vicinity of the control rod regions and the interfaces between the MOX and UOX assemblies, which is usually difficult to capture the good numerical solutions due to the strong heterogeneity and complicated material distribution.

To further demonstrate the capability of the accelerated SDUGKS in capturing the sharp changes of scalar fluxes and powers, Figs. 14 and 15 present the power densities and the fast-group scalar fluxes of the accelerated SDUGKS and the reference solutions along the vertical centerline. The reference solutions are obtained by the S_N method with the diamond difference method on the fine mesh size of 0.252 cm×0.252 cm

TABLE VII. Effective multiplication factor for the full core UOX/MOX pin-by-pin system (cell size: 1.26 cm×1.26 cm).

	Effective multiplication factor		
Core	SDUGKS	Reference	Relative error
A	1.014793	1.014338	0.0004486
B	0.998879	0.998911	0.0000320
C	1.002728	1.002609	0.0001187
D	1.000582	1.000503	0.0000790

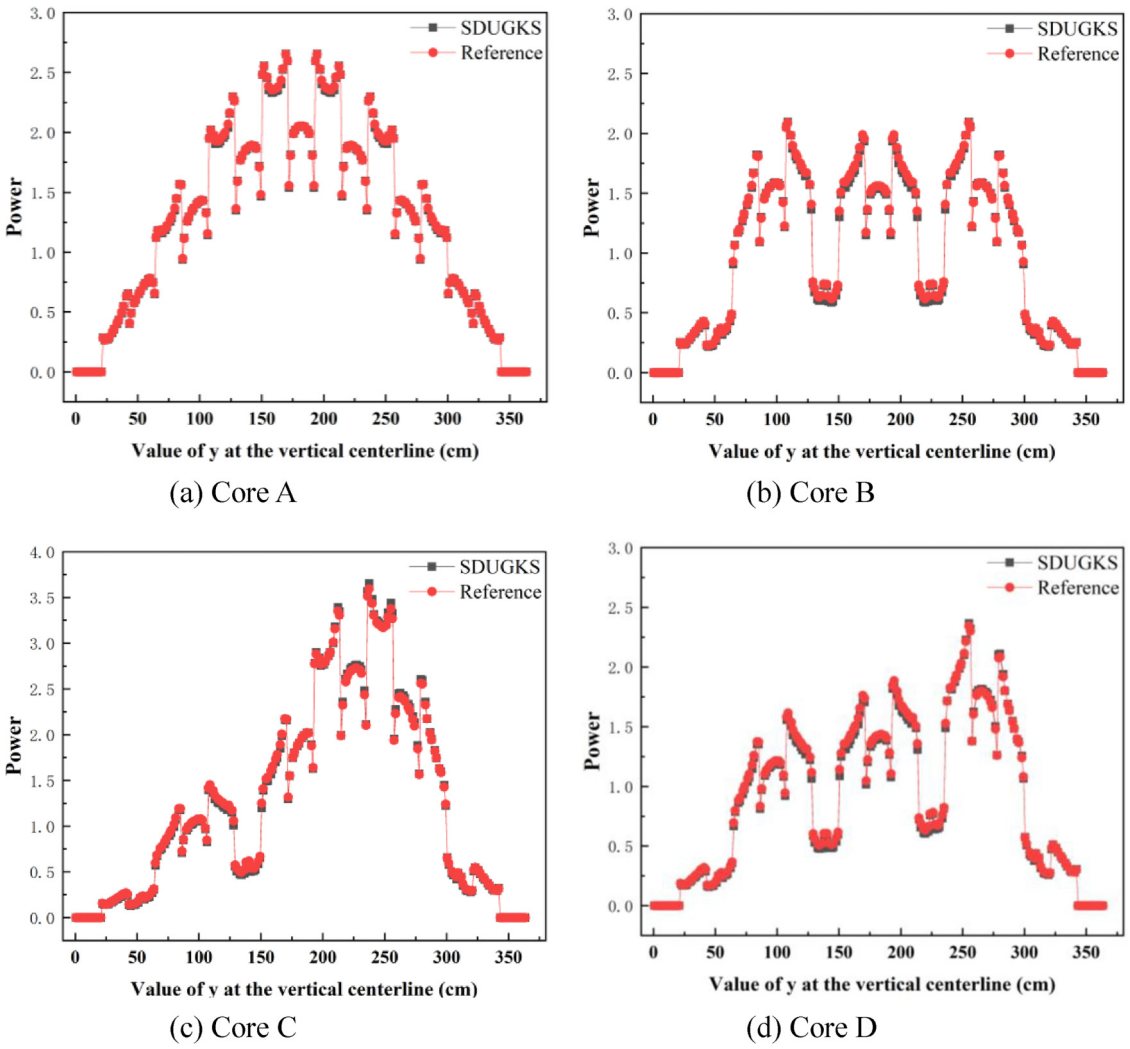

FIG. 14. Results of pin-by-pin power density along the vertical centerline (cell size: 1.26 cm×1.26 cm).

(5×5 nodes per pin cell). The effective multiplication factors and relative errors are given in Table VII. It can be found that the results of the accelerated SDUGKS agree well with the reference solutions for this complicated pin-by-pin high-resolution reactor system, which demonstrates again the capability of the proposed accelerated SDUGKS for multiscale neutron transport problems.

Figure 16 and Table VIII present the iterative convergence properties of the accelerated SDUGKS. For the original SDUGKS, obvious differences in the outer iterative steps can be observed, ranging from 519 to 1829, for the four cases due to the influence of the control rods inserted. However, for the accelerated SDUGKS, the outer iterative numbers are the same (27 steps) for all cases, which can be attributed to the robust acceleration of the macroscopic coarse mesh acceleration. The speedups in terms of CPU time for the accelerated SDUGKS reach to 18.70, 14.76, 50.82, and 62.95, respectively. Furthermore, the CPU time of the macroscopic coarse mesh acceleration computation is far less than the total time of the accelerated SDUGKS. The speedup in terms of

TABLE VIII. Acceleration analysis of the full core UOX/MOX pin-by-pin homogeneous models (cell size: 1.26 cm×1.26 cm).

			Accelerated SDUGKS				
	SDUGKS		Time (s)			Speedup	
Core	Time (s)	Steps	SDUGKS	Macroscopic coarse mesh	Steps	Time	Steps
A	20143.51	519	1041.26	36.1434	27	18.70	19.22
B	15684.55	412	1027.77	34.5434	27	14.76	15.26
C	56175.41	1377	1036.08	69.3000	27	50.82	51.00
D	73788.90	1829	1091.42	80.7591	27	62.95	67.74

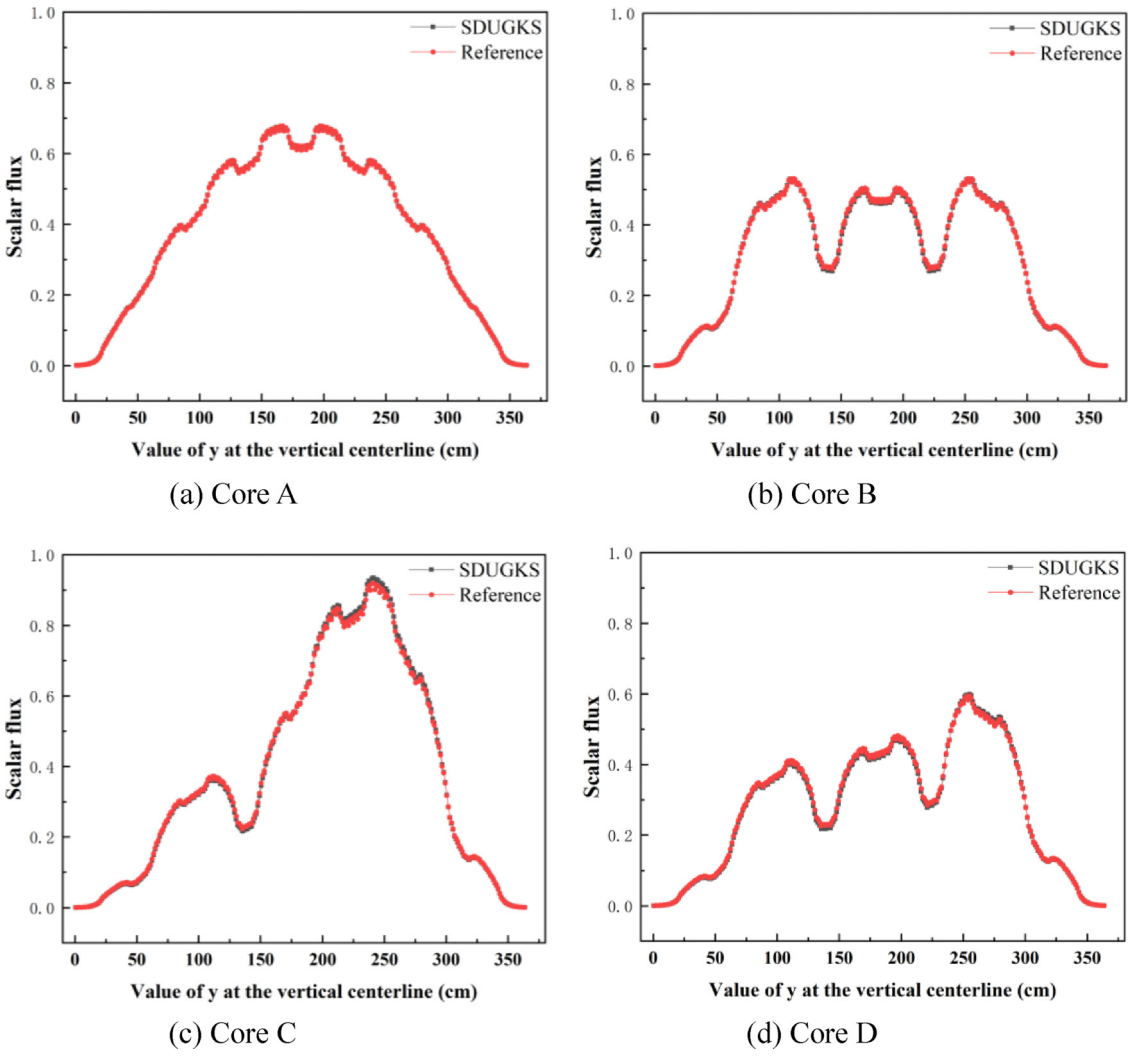

FIG. 15. Results of fast-group scalar fluxes along the vertical centerline (cell size: 1.26 cm×1.26 cm).

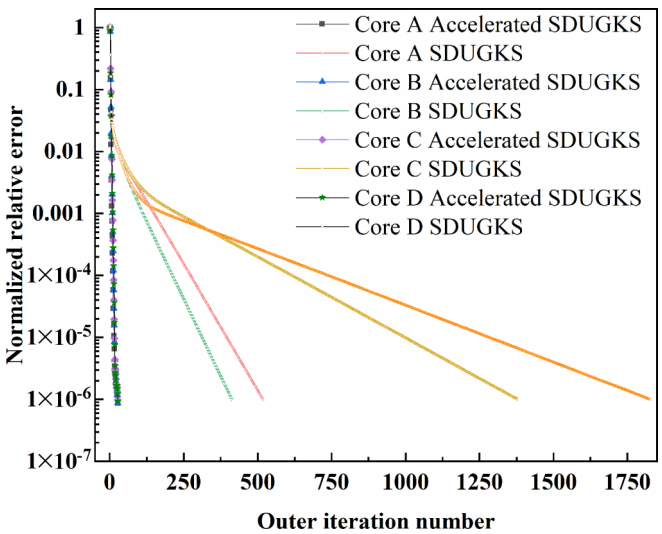

FIG. 16. Convergence history of the original SDUGKS and accelerated SDUGKS for the full core UOX/MOX pin-by-pin system.

CPU time is nearly the same as that of the iterative steps, which further verifies the acceleration performance of the accelerated SDUGKS for large-scale and complicated practical engineering transport problems.

IV. CONCLUSION

In this paper, an accelerated multiscale discrete unified gas kinetic scheme (accelerated SDUGKS) is developed for steady neutron transport, in which the macroscopic coarse mesh acceleration technique is employed to improve the convergence of the SDUGKS for an optically thick system. With the introduction of the macroscopic governing equations derived from the moment equations of the NBTE and the latest SDUGKS, the numerical solution of the NBTE on fine meshes at the mesoscopic level can be rapidly obtained. Furthermore, the use of the coarse mesh based on the Krylov subspace method for the macroscopic governing equation can reduce the computational variables in comparison with those of the NBTE on the fine mesh at the mesoscopic level, which greatly improves the computational efficiency of the macroscopic coarse mesh acceleration technique.

The numerical accuracy and the acceleration properties are validated by the several typical assembly-wise and more complicated pin-by-pin full core multiscale neutron transport problems based on realistic reactor geometry and data. In further work, we will extend the proposed accelerated SDUGKS to other particle transport problems.

ACKNOWLEDGMENTS

This work was supported by the National Natural Science Foundation of China (Grant No. 12005073) and the National Key R&D Program of China (Grant No. 2020YFB1901600).

[1] Y. Azmy and E. Sartori, *Nuclear Computational Science: A Century in Review* (Springer Science & Business Media, Berlin, 2010).

[2] D. G. Cacuci, *Handbook of Nuclear Engineering* (Springer Science & Business Media, Berlin, 2010).

[3] P. K. Romano, N. E. Horelik, B. R. Herman, A. G. Nelson, B. Forget, and K. Smith, OpenMC: A state-of-the-art Monte Carlo code for research and development, Ann. Nucl. Energy **82**, 90 (2015).

[4] W. F. Miller and E. E. Lewis, *Computational Methods of Neutron Transport* (American Nuclear Society, La Grange Park, Illinois, 1993).

[5] S. P. Hamilton and T. M. Evans, Efficient solution of the simplified P_N equations, J. Comput. Phys. **284**, 155 (2015).

[6] G. Marleau, DRAGON theory manual Part 1: Collision probability calculations, Technical Report IGE-236 Rev 1, 2001.

[7] E. W. Larsen, B. Collins, B. Kochunas, A. Graham, and S. Stimpson, *MPACT Theory Manual Version 4.3* (No. ORNL/SPR-2021/2330) (Oak Ridge National Laboratory, Oak Ridge, TN, 2022).

[8] K. D. Lathrop and F. W. Brinkley, *TWOTRAN-II: An Interfaced, Exportable Version of the TWOTRAN Code for Two-Dimensional Transport* (No. LA-4848-MS) (Los Alamos Scientific Laboratory, New Mexico, 1973).

[9] T. M. Evans, A. S. Stafford, R. N. Slaybaugh, and K. T. Clarno, Denovo: A new three-dimensional parallel discrete ordinates code in SCALE, Nucl. Technol. **171**, 171 (2010).

[10] Z. L. Guo, R. Wang, and K. Xu, Discrete unified gas kinetic scheme for all Knudsen number flows. II. Thermal compressible case, Phys. Rev. E **91**, 033313 (2015).

[11] L. H. Zhu, S. Z. Chen, and Z. L. Guo, dugksFoam: An open source OpenFOAM solver for the Boltzmann model equation, Comput. Phys. Commun. **213**, 155 (2017).

[12] Y. J. Zhu, C. W. Zhong, and K. Xu, An implicit unified gas-kinetic scheme for unsteady flow in all Knudsen regimes, J. Comput. Phys. **386**, 190 (2019).

[13] W. J. Sun, S. Jiang, and K. Xu, An asymptotic preserving unified gas kinetic scheme for gray radiative transfer equations, J. Comput. Phys. **285**, 265 (2015).

[14] Z. L. Guo and K. Xu, Discrete unified gas kinetic scheme for multiscale heat transfer based on the phonon Boltzmann transport equation, Int. J. Heat Mass Transfer **102**, 944 (2016).

[15] H. T. Liu, F. Shi, J. Wan, X. M. He, and Y. Cao, Discrete unified gas kinetic scheme for a reformulated BGK–Vlasov–Poisson system in all electrostatic plasma regimes, Comput. Phys. Commun. **255**, 107400 (2020).

[16] S. Tan, W. J. Sun, J. X. Wei, and G. X. Ni, A parallel unified gas kinetic scheme for three-dimensional multi-group neutron transport, J. Comput. Phys. **391**, 37 (2019).

[17] X. F. Zhou and Z. L. Guo, Discrete unified gas kinetic scheme for steady multiscale neutron transport, J. Comput. Phys. **423**, 109767 (2020).

[18] E. W. Larsen, J. E. Morel, and W. F. Miller, Asymptotic solutions of numerical transport problems in optically thick, diffusive regimes, J. Comput. Phys. **69**, 283 (1987).

[19] L. Miecussens, On the asymptotic preserving property of the unified gas kinetic scheme for the diffusion limit of linear kinetic models, J. Comput. Phys. **253**, 138 (2013).

[20] Z. L. Guo, J. Q. Li, and K. Xu, Unified preserving properties of kinetic schemes, Phys. Rev. E **107**, 025301 (2023).

[21] M. L. Adams and E. W. Larsen, Fast iterative methods for discrete-ordinates particle transport calculations, Prog. Nucl. Energy **40**, 3 (2002).

[22] R. E. Alcouffe, Diffusion synthetic acceleration methods for the diamond-differenced discrete-ordinates equations, Nucl. Sci. Eng. **64**, 344 (1977).

[23] M. Bando, T. Yamamoto, Y. Saito, and T. Takeda, Three-dimensional transport calculation method for eigenvalue problems using diffusion synthetic acceleration, J. Nucl. Sci. Technol. **22**, 841 (1985).

[24] G. L. Ramone, M. L. Adams, and P. F. Nowak, A transport synthetic acceleration method for transport iterations, Nucl. Sci. Eng. **125**, 257 (1997).

[25] K. S. Smith, Nodal method storage reduction by nonlinear iteration, Trans. Amer. Nucl. Soc. **44**, 265 (1983).

[26] N. Z. Cho, G. S. Lee, and C. J. Park, Partial current-based CMFD acceleration of the 2D/1D fusion method for 3D whole-core transport calculations, Trans. Amer. Nucl. Soc. **88**, 594 (2003).

[27] L. L. Li, *A Low Order Acceleration Scheme for Solving the Neutron Transport Equation*, Doctoral Dissertation (Massachusetts Institute of Technology, Cambridge, MA, 2013).

[28] A. Zhu, M. Jarrett, Y. L. Xu, B. Kochunas, E. Larsen, and T. Downar, An optimally diffusive coarse mesh finite difference method to accelerate neutron transport calculations, Ann. Nucl. Energy **95**, 116 (2016).

[29] G. R. Cefus and E. W. Larsen, Stability analysis of coarse-mesh rebalance, Nucl. Sci. Eng. **105**, 31 (1990).

[30] A. Yamamoto, Generalized coarse-mesh rebalance method for acceleration of neutron transport calculations, Nucl. Sci. Eng. **151**, 274 (2005).

[31] P. F. Nowak, E. W. Larsen, and W. R. Martin, A multigrid method for S_N calculations in x-y geometry, Trans. Amer. Nucl. Soc. **56**, 291 (1988).

[32] L. R. Cornejo and D. Y. Anistratov, Nonlinear diffusion acceleration method with multigrid in energy for k-eigenvalue neutron transport problems, Nucl. Sci. Eng. **184**, 514 (2016).

[33] S. Oliveira and Y. Deng, Preconditioned Krylov subspace methods for transport equations, Prog. Nucl. Energy **33**, 155 (1998).

[34] T. Mazumdar and A. Gupta, Application of Krylov acceleration technique in method of characteristics-based neutron transport code, Nucl. Sci. Eng. **192**, 153 (2018).

[35] J. Willert, H. Park, and D. A. Knoll, A comparison of acceleration methods for solving the neutron transport k-eigenvalue problem, J. Comput. Phys. **274**, 681 (2014).

[36] B. G. Carlosn and C. E. Lee, *Mechanical Quadrature and the Transport Equation* (Los Alamos Scientific Laboratory of the University of California, Walnut Creek, 1961), Vol. 2573.

[37] W. M. Stacey, *Nuclear Reactor Physics* (Wiley, New York, 2018).

[38] L. Gianluca, Advanced quadrature sets and acceleration and preconditioning techniques for the discrete ordinates method in parallel computing environments, Doctoral dissertation (University of Florida, Gainesville, 2004).

[39] X. F. Zhou, C. M. Zhong, and Y. Y. Zhang, Jacobian-free Newton Krylov two-node coarse mesh finite difference based on nodal expansion method for multiphysics coupled models, Ann. Nucl. Energy **168**, 108915 (2022).

[40] T. F. Chan and H. A. Van Der Vorst, *Approximate and Incomplete Factorizations* (Springer, Netherlands, 1997).

[41] Y. Saad, *Iterative Methods for Sparse Linear Systems* (SIAM, Philadelphia, 2003).

[42] A. C. Center, *Benchmark Problem Book: ANL-7416, Supplement 2 (Computational Benchmark Problems Committee of the Mathematics and Computation Division)* (American Nuclear Society, Illinois, 1977).

[43] H. K. Louis, Investigation of the IAEA benchmark problem using MCNP code, Arab J. Nucl. Sci. Appl. **52**, 169 (2019).

[44] A. Cherezov, R. Sanchez, and H. G. Joo, A reduced-basis element method for pin-by-pin reactor core calculations in diffusion and SP3 approximations, Ann. Nucl. Energy **116**, 195 (2018).

[45] X. F. Zhou, Jacobian-free Newton Krylov two-node coarse mesh finite difference based on nodal expansion method, Nucl. Eng. Technol. **54**, 3059 (2022).

[46] C. Cavarec, J. F. Perron, D. Verwaerde, and J. P. West, *Benchmark Calculations of Power Distribution within Assemblies* (No. NEA-NSC-DOC–94-28) (Nuclear Energy Agency, 1994).